Effects of elemental ratios in CZTSe film on CZTSe/CdS band alignment and inhomogeneity in absorber thermal conductivity

Qiong Chen [a], and Yong Zhang [a]

[a] Department of Electrical and Computer Engineering, and Energy Production and Infrastructure Center (EPIC), The University of North Carolina at Charlotte, Charlotte, NC 28223, USA

Abstract — **CZTSe solar cells with different elemental ratios are compared for their photo-response with low and high illumination densities. Elemental ratios are found not only affecting the defect density, but also Mo/CZTSe/CdS band alignment. Higher Sn/Cu and lower Zn ratio was found more immune to EQE droop at high power illumination, although it yields lower EQEs at low power level. Furthermore, inhomogeneity in thermal conductivity was found within the film. The findings suggest the potential to modify Zn and Sn ratios adapting to different operation conditions and applications.**

I. INTRODUCTION

It is well-recognized that elementary ratios of Cu, Zn, Sn, S(Se) within CZTS(Se) absorber layer can have great impact on the CZTS(Se) solar cell performance. It has been found empirically that Cu-poor and Zn-rich condition tends to offer better performance than stoichiometry, which has been explained as that the stoichiometry condition prompts point defect formation [1-5]. In this work, by comparing the spatially-resolved photo-responses of CZTSe solar cells with different elemental ratios under different illumination conditions, we have found that when illuminated at high power density, the cell with elemental ratios closer to stoichiometry is more immune to EQE droop than that more off-stoichiometry. The finding indicates that the variation in elemental ratios does not simply result in less or more defects, but also changes the band alignment at the absorber-back contact and/or absorber-window layer interface(s). The latter effect is perhaps more significant for the better performance of the off-stoichiometry cell, but it might not necessarily be a wise option for achieving further improved performance.

II. EXPERIMENTAL DETAILS

μ-Raman measurement was performed with a Horiba Jobin Yvon HR800 confocal Raman system with a CCD detector using a 532 nm laser. With a 100x objective lens, whose numerical aperture is 0.9, the diffraction limit laser spot size is ~0.72 μm. μ-LBIC measurements were performed using the same system [6]Two gold plated probes are used to carry the LBIC from the solar cell to a current pre-amplifier (SR570) followed by a lock-in amplifier (SR830). With the help of a Si reference cell (PV Measurements, Inc.), the LBIC data were converted into external quantum efficiencies (EQEs). Macroscopic I-V curves were obtained by Keithley 4200 with uniform near 1 sum illumination (985 W/m^2).

CZTSe devices M3690_13 and M3652_13 used in this work are similar to those reported in Ref. [3]. The CZTSe films were grown by a co-evaporation method with different film thickness and elemental ratios, as summarized in table I. The standard device structure and device fabrication are described in Ref. [3]., Different from the standard structure, a 150 Å E-beam evaporated NaF precursor was omitted before absorber deposition in both of the samples used in this work.

III. RESULTS AND DISCUSSIONS

μ-LBIC mappings were performed with 532 nm laser at both low (~2 μW; 5 x 10^2 W/cm^2) and high laser power (~ 179 μW; 4.5 x 10^4 W/cm^2) levels to examine the photo-response in different illumination conditions. By "lower power", we mean the power level that can yield an average EQE comparable to the macroscopic probe, whereas by "high power" the EQE of the general area shows significant degradation, but the power is not as high as to cause permanent damage to the material.

For M3690_13 with 4% efficiency, the average EQE at ~2μW with 532 nm laser is 50%±0.3%. Histogram of the LBIC mapping in Fig. 1(c) shows that the majority part of the mapped region exhibits high EQEs from 45% to 55%. However, at higher power level, the general area of M3690_13 experienced drastic, about 85%, EQE droop, similar with the results reported in Ref. [6]. With only ~ 3% cell efficiency, the average EQE of M3652_13 is 58.4% at low power level. One should be noted that due to thicker absorber, M3690_13 yield a slight lower average EQE at 532 nm than M3652_13. However, the average EQE of M3690_13 at 633 nm is higher than that of M3652_13. The interesting result comes from the EQEs of M3652_13 at the high power level illumination condition. As shown in Fig. 2(b), at ~179 μW, the average EQE of M 3652_13 is 55.7%, thus

TABLE I
COMPARISON OF CZTSe DEVICES

	Absorber thickness	Zn/Sn	Cu/(Zn+Sn)	Efficiency	Fill Factor	I$_{SC}$	V$_{OC}$
M3690_13	2.09 μm	1.41	0.85	4.06%	46.8%	13.4 mA	268 mV
M3652_13	1.54 μm	1.12	0.97	2.68%	42.4%	9.47 mA	276 mV

there was almost no EQE droop, although it did occur at even higher power (to be discussed layer). Comparing the histograms in Figs. 2(c) and (d), the result at high power is very similar with that at low power.
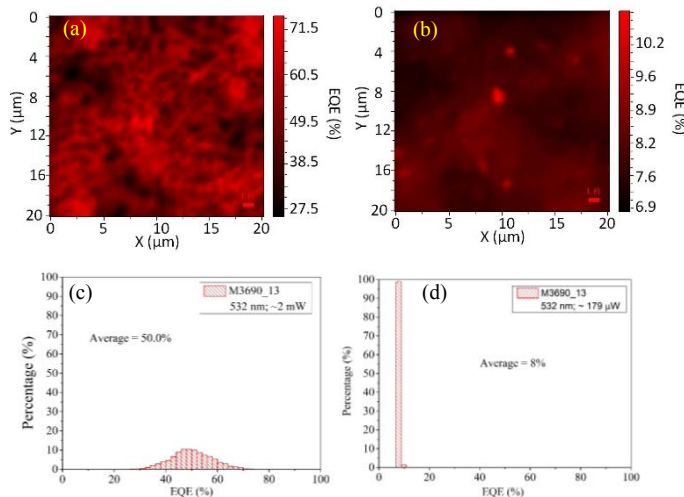

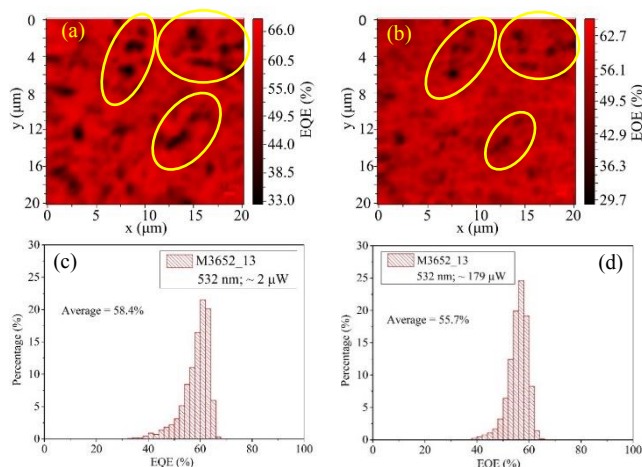Fig. 1.   M3690_13 LBIC mapping with 532 nm laser at low and high power levels: (a) at ~ 2 µW; (b) at ~ 179 µW; (c) histogram of (a); (d) histogram of (b).

Fig. 2.   M3652_13 LBIC mapping with 532 nm laser at low and high power levels: (a) at ~ 2 µW; (b) at ~ 179 µW; (c) histogram of (a); (d) histogram of (b).

Raman spectra obtained from randomly selected general spots from the two CZTSe devices are compared. Main peaks in all spectra are 172 cm^{-1} and 196 cm^{-1} from CZTSe, and 303 cm^{-1} from CdS with similar intensities. It indicates there is no significant difference in the CdS layer thickness between the devices. In other words, it was not the variation in CdS layer thickness that led to the different EQE droops when illuminated at high power level. One obvious difference between M3652_13 and M3690_13 is the Cu/(Zn+Sn) and Zn/Sn ratios in the absorber. The difference in the elemental ratios are likely to be the main reason that results in the different illumination density dependence between the devices. For M3652_13, lower

short circuit current, efficiency and EQE were indeed observed from its macroscopic I-V curve as well as low power illumination LBIC mapping. Therefore, with a higher Cu/(Zn+Sn) ratio and a lower Zn/Sn ratio in M3652_13, one might naturally consider that the lower efficiency of M3652_13 could be mainly caused by the defect problems associated with the unfavorable close to stoichiometry condition, if one only considers the low illumination density results. However, if we take into account the illumination power density dependence, the answer cannot be so simple! One normally expects that the adverse effect of the point defects, e.g., Sn$_{Zn}$, will be at least partially eliminated at high excitation density, at least more so for the off-stoichiometry sample, because the point defects are relatively easy to be saturated [7].

Besides the possible defect mitigation effect invoked in the literature, our finding seems to suggest that changing Cu/(Zn+Sn) and Zn/Sn ratios could have another important effect on the device performance, that is, affecting the band alignment of the CZT(S,Se)/CdS heterostructure. CdS/CZTSe is mostly found to have a "spike" like alignment, in which the conduction band minimum (CBM) of CdS is higher than that of CZTSe. Type I alignment benefits in V$_{OC}$ but becomes a barrier for carriers moving across the heterojunction. Increasing Zn/Sn ratio is expected to increase the CBM of CZTSe, which is beneficial for the electron collection. Thus CZTSe devices with higher Zn/Sn and lower Cu/(Zn+Sn) ratios usually yield better photo-response. However, when illuminated with high power density, raising of the electron Fermi level might lower the electron barrier at the back contact, thus, allowing electrons to leak out through the back contact. Thus, materials with higher Cu and lower Zn content, expected to have higher Mo back electron blocking barrier, could still generate a relatively high EQE at high power illumination, although the initial I$_{SC}$ was lower at low illumination density, because of unfavorable band alignment between CZTSe and CdS.

LBIC mapping from another random region (Fig. 3(a)) of M3652_13 was obtained first illuminated with ~ 2 µW, then with high power ~ 2.47 µW. At ~ 2 µW, the average EQE is also very low, around 47%. At ~ 2.47 mW, LBIC mapping of M3652_13 showed large inhomogeneity in Fig. 3(d), with an average of 6.9% and a maximum EQE of 15.6% and minimum of 1.8%. An optical image taken after the 2.47 mW LBIC mapping is shown as Fig. 3(c), where one area (upper left) exhibits apparent color change with the shape and position of the region matching the lower EQE region in Fig. 3(d). ~ 2 µW LBIC mapping was performed again at the same region, as shown in Fig. 3(e). The upper left part of the mapping area yields EQE as small as 1%. However, the lower right part still generates EQEs which are comparable to the EQEs of the first ~ 2 µW LBIC mapping. Thus, this part of the absorber was only slightly or not affected by the rather high power ~ 2.47 mW illumination, while the properties of the left part film was severely changed due to the high power illumination. Similar LBIC mapping was also performed with M3690_13. At ~ 2.45 mW illumination, EQE of M3690_13 dropped almost a factor

of twenty, and the entire illuminated region could not recover when illuminated by ~ 2 µW again. This comparison suggests that areas similar to the lower right region in Fig. 3(d) on M3652_13 are much more immune to very high illumination density than absorber of M3690_13.
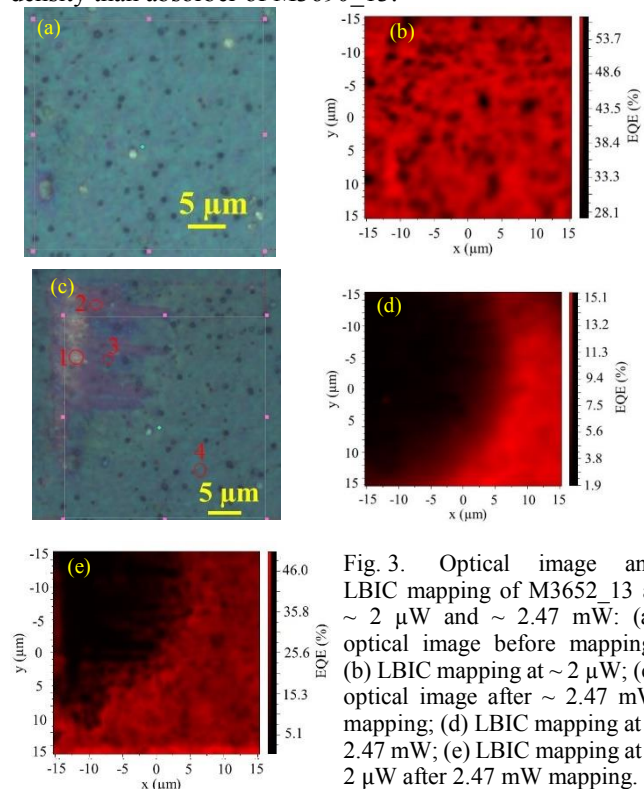

Fig. 3. Optical image and LBIC mapping of M3652_13 at ~ 2 µW and ~ 2.47 mW: (a) optical image before mapping; (b) LBIC mapping at ~ 2 µW; (c) optical image after ~ 2.47 mW mapping; (d) LBIC mapping at ~ 2.47 mW; (e) LBIC mapping at ~ 2 µW after 2.47 mW mapping.

Raman spectroscopy was performed at different spots from the mapping regions of M3652_13 to analyze the composition differences between the spots showing different colors. Raman spectra at 179 µW were collected from four different spots numbered 1- 4 and circled in Fig. 3(c), and one additional random spot outside the mapped area. In Fig. 4, spot 1, which has a color lighter than its original, showed very strong t-Se modes at 238 cm^{-1}, and second and third resonant modes at 477 and 714 cm^{-1}, respectively. The dominant Raman component for spots like spot 1 has become t-Se [8], which suggests degradation of CZTSe after ~ 2.47 mW illumination. For spot 2, the most significant change was the redshifts of the CZTSe and CdS main peak, line width broadening, and intensity drop caused by heating effect. And for the spot 3, the mesa like band from 220 to 250 cm^{-1} had become narrower and become a band centered near 238 cm^{-1}. All the three types of spot experienced EQE droop after ~ 2.45 mW illumination. However, other spots like the spot 4, still yields EQE around 30% to 40% afterward. And the Raman spectrum of the spot 4 is very similar with that of the random spot, indicating no structure or composition change after ~ 2.47 mW illumination. Such different behavior of these spots after ~ 2.47 mW illumination may indicate the large inhomogeneity of thermal conductivity within the film. If the entire device area can be manufactured the same with the regions which are relatively more immune to high power

illumination, CZTSe may have a potential in concentrated PV application.
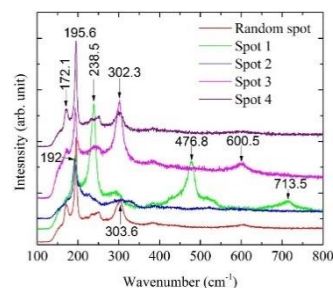

Fig. 4. Raman spectra comparison of different spots from M3652_13 surface after 2.47 mW LBIC mapping.

IV. CONCLUSIONS

CZTSe device with a higher Sn/Cu and lower Zn ratio generates lower Isc and efficiency at low power level. However, at high power level illumination, it can still yield EQEs comparable to EQEs at low power level. Our findings suggest that the elemental ratios in CZTSe absorber may change the electronic barrier at the absorber-back contact and/or absorber-window layer interface(s). It also points out the possibility to modify the tin and zinc ratios adapting to different device operation conditions and applications.

ACKNOWLEDGEMENT

REFERENCES

[1] W. Wang, M. T. Winkler, O. Gunawan, T. Gokmen, T. K. Todorov, Y. Zhu, *et al.*, "Device Characteristics of CZTSSe Thin-Film Solar Cells with 12.6% Efficiency," Advanced Energy Materials, vol. 4, 2014.
[2] T. K. Todorov, K. B. Reuter, and D. B. Mitzi, "High-Efficiency Solar Cell with Earth-Abundant Liquid-Processed Absorber," Advanced materials, vol. 22, pp. E156-E159, 2010.
[3] I. Repins, C. Beall, N. Vora, C. DeHart, D. Kuciauskas, P. Dippo, *et al.*, "Co-evaporated Cu 2 ZnSnSe 4 films and devices," Solar Energy Materials and Solar Cells, vol. 101, pp. 154-159, 2012.
[4] H. Katagiri, K. Jimbo, W. S. Maw, K. Oishi, M. Yamazaki, H. Araki, *et al.*, "Development of CZTS-based thin film solar cells," Thin Solid Films, vol. 517, pp. 2455-2460, 2009.
[5] S. Chen, L.-W. Wang, A. Walsh, X. Gong, and S.-H. Wei, "Abundance of CuZn+ SnZn and 2CuZn+ SnZn defect clusters in kesterite solar cells," Applied Physics Letters, vol. 101, p. 223901, 2012.
[6] Q. Chen and Y. Zhang, "The reversal of the laser-beam-induced-current contrast with varying illumination density in a Cu2ZnSnSe4 thin-film solar cell," Applied Physics Letters, vol. 103, p. 242104, 2013.
[7] T. Gfroerer, Y. Zhang, and M. Wanlass, "An extended defect as a sensor for free carrier diffusion in a semiconductor," Applied Physics Letters, vol. 102, p. 012114, 2013.
[8] V. V. Poborchii, A. V. Kolobov, and K. Tanaka, "An in situ Raman study of polarization-dependent photocrystallization in

amorphous selenium films," Applied physics letters, vol. 72, p. 1167, 1998.